Effects of Nonlinear Diode Junction Capacitance on the Nose-to-Nose Calibration

Kate A. Remley, *Member, IEEE*, Dylan F. Williams, *Senior Member, IEEE*, Donald C. DeGroot, *Senior Member, IEEE*, Jan Verspecht, and John Kerley, *Member, IEEE*

***Abstract*—We examine the effects of nonlinear diode junction capacitance on the fundamental premise of the nose-to-nose calibration, that the kickout pulse is identical in shape and duration to the impulse response of a sampling circuit. We offer a physical explanation for the error introduced by the nonlinear junction capacitance using small-signal diode equations.**

***Index Terms*—Digital sampling oscilloscope, nose-to-nose calibration, phase error, samplers.**

I. Introduction

In this letter, we show how nonlinear diode junction capacitance generates errors in the "nose-to-nose" calibration technique [1]–[3]. This calibration provides an estimate of the response of a broadband sampling oscilloscope, and can be used to correct measurements made with the oscilloscope. The fundamental premise of the nose-to-nose calibration is that the sampler "kickout" pulse, which is generated at the input port of a two-diode sampling circuit when a dc offset is applied to the diode bias, is identical in shape to the sampler's time-domain "impulse response" [4].

While the error of the nose-to-nose calibration magnitude response can be estimated from power measurements of a swept-sine source [5], our options for finding the phase error are currently restricted to computational methods. [2], [3] develop an analytic model for the sampling circuit which shows that the fundamental nose-to-nose premise holds for samplers consisting of diodes with constant junction capacitance embedded in a linear network. A recent analytic method extends these models to include nonlinear diode junction capacitance [6].

Here we use numerical methods to efficiently examine many aspects of the sampling circuit behavior. We use a realistic model of a sampling circuit in SPICE, and derive a small-signal model from the large-signal behavior of the circuit. We show that the nonlinear capacitance introduces errors not accounted for in current practice, and offer a physical explanation for these errors in terms of small-signal diode equations.

Manuscript received October 31, 2000; revised February 17, 2001. The review of this letter was arranged by Associate Editor Dr. Arvind Sharma.

K. A. Remley, D. F. Williams, and D. C. DeGroot are with the RF Technology Division 813.01, National Institute of Standards and Technology, Boulder, CO 80305-3328 USA.

J. Verspecht is with Agilent Technologies, Inc., Brussels 1050, Belgium.

J. Kerley is with the Agilent Technologies, Inc., Colorado Springs, CO 90901-2197 USA.

Publisher Item Identifier S 1531-1309(01)04010-7.

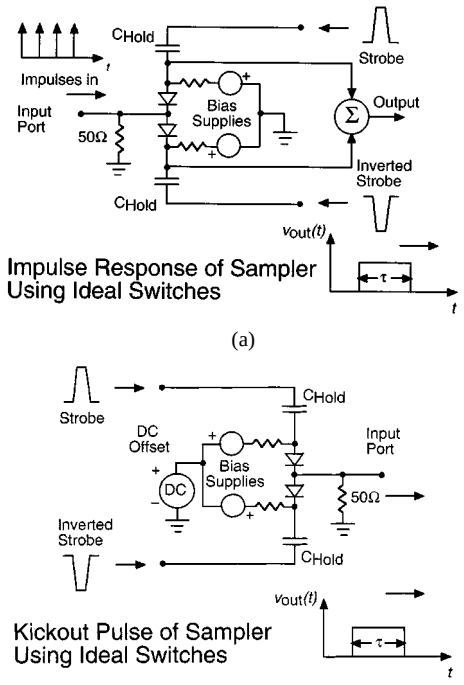

Fig. 1. (a) Impulse response and (b) kickout pulse generation for a simple two-diode sampler.

II. Nose-to-Nose Calibration

We describe important aspects of the nose-to-nose calibration and describe an intuitive way to understand the fundamental premise of the calibration using an ideal sampler. We then extend this description to the realistic case.

A. The Sampling Circuit

A simplified representation of the sampling circuit we analyzed is shown in Fig. 1. It is based on a model for a 20-GHz oscilloscope [7], [8]. The simplified output circuit consists of a charge amplifier that sums the charge stored on the hold capacitors during each sampling cycle, as shown in Fig. 1(a).

The strobe signal forward biases the diodes during each sampling cycle. Because the strobe appears differentially across the output amplifier, its effects cancel at the output. When a nonzero voltage exists at the input port and the diodes are forward biased, a net charge proportional to the input voltage will transfer through the diodes to the hold capacitors. If the input and strobe signals are periodic and the strobe's period is slightly different than that of the input, a representation of the input signal will eventually be traced out by the digitized voltage samples.

U.S. Government work not protected by U.S. copyright

B. Impulse Response

We define the digitized output of the sampler in response to periodic excitation by Dirac delta functions as the "impulse response" of the sampler. For small-signal inputs, the output of the sampler can be represented by the convolution of this impulse response and the input signal [4]. Currently, we have no way to directly measure this impulse response, in part because we are unable to generate infinitely sharp or perfectly characterized pulses. However, we can derive an estimate of the impulse response of the sampler using the nose-to-nose calibration.

C. Kickout Pulse

When we apply a dc offset voltage to the bias lines of the diodes, the hold capacitors charge when the diodes are reversed biased. Each time the strobe fires, the discharging hold capacitors create a pulse that appears at the input port of the sampler. This "kickout" pulse ideally will be the same duration as the impulse response, but scaled in amplitude by some constant [1].

D. Nose-to-Nose Premise

This premise, that the kickout pulse is identical in shape and duration to the impulse response, can be illustrated clearly if we imagine replacing the diodes by ideal switches. The impulse response of a sampler constructed with ideal switches and with small-signal, ideal impulse excitation, is a rectangular pulse[1]. The duration of the pulse is the same as that of the switch closure [Fig. 1(a)]. We generate kickout pulses on a second ideal-switch sampler by replacing the impulse excitation with a dc offset on the bias lines. Each time the strobe fires, a pulse of the same duration as the switch closure appears at the input port of the sampler [Fig. 1(b)].

If we connect the input ports of our two ideal-switch samplers together (nose-to-nose), the output will be the convolution of the rectangular kickout and the rectangular impulse response. This convolution, a triangular waveform of duration 2τ, is what we would measure at the output of the second sampler. A simple deconvolution process gives us τ, from which we can find the impulse response.

When the ideal switches are replaced by diodes, the impulse response is no longer a simple rectangular function, but is altered by both the conductance and the junction capacitance of the diodes. Nevertheless, the procedure still works if the normalized kickout and impulse responses are the same.

We can estimate the frequency-domain representation of the impulse response of one sampler as the square root of the output response of the second sampler. That is

$$H_A(\omega)^{\text{est}} \cong \sqrt{K_B(\omega)H_A(\omega)} \tag{1}$$

where

- H_A frequency-domain representation of the impulse response of sampler A;
- K_B frequency-domain representation of the kickout pulse emanating from sampler B;
- ω angular frequency.

[1]This pulse is rectangular when the RC time constant of the circuit resistance and the hold capacitor is much longer than the duration of the sampling window. This condition is true for the sampling circuits we investigated.

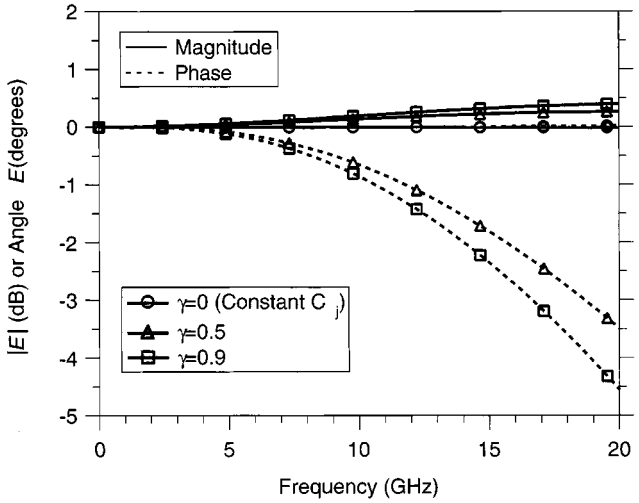

Fig. 2. Increase in the error ratio E of the nose-to-nose calibration for a 20-GHz sampling circuit with increasing nonlinearity in the diode's junction capacitance.

If $K(\omega)$ is directly proportional to $H(\omega)$, and $H_A(\omega) = H_B(\omega)$, then $H_A(\omega)^{\text{est}} = \text{C}H_A(\omega)$, where C is a proportionality constant.

Because no two samplers are identical, in practice the estimate of the impulse response of sampler A is found from a set of three measurements of three samplers. However, the calibration is still based upon the assumption that the kickout is proportional to the impulse response for each sampler. Therefore, we define the error ratio E for a sampler response estimate as

$$E(\omega) \equiv \frac{H_A^{\text{est}}(\omega)}{H_A(\omega)} \cong \frac{\sqrt{K_B(\omega)H_A(\omega)}}{H_A(\omega)} = \sqrt{\frac{K_B(\omega)}{H_A(\omega)}}. \tag{2}$$

III. Simulation Results

We implemented the 20-GHz sampling circuit described in [7], [8] in SPICE, neglecting any packaging parasitics, input networks, or filtering at the input of the sampler in order to concentrate on the effect of the nonlinear capacitance. We used a common model for a Schottky-barrier diode [8], [9] in which the diode conductance is in parallel with a time-varying, voltage-dependent junction capacitance. In this model, the diode's junction capacitance, $C(V_j)$, is given by

$$C(V_j) = \frac{C_{j0}}{(1-(V_j(t)/\phi_{\text{bi}}))^{\gamma}} \tag{3}$$

where

- C_{j0} zero-voltage junction capacitance;
- V_j large-signal, time-varying voltage across the diode's junction;
- ϕ_{bi} junction's built-in potential;
- γ grading coefficient.

The grading coefficient sets the amount of nonlinearity in the junction capacitance, and is typically around $\gamma = 0.5$ for the type of Schottky-barrier diodes used in modern samplers [9].

Fig. 2 shows an increase in the error of the nose-to-nose calibration as we increase the nonlinearity in the diode's junction capacitance in our 20-GHz sampling circuit model. The results

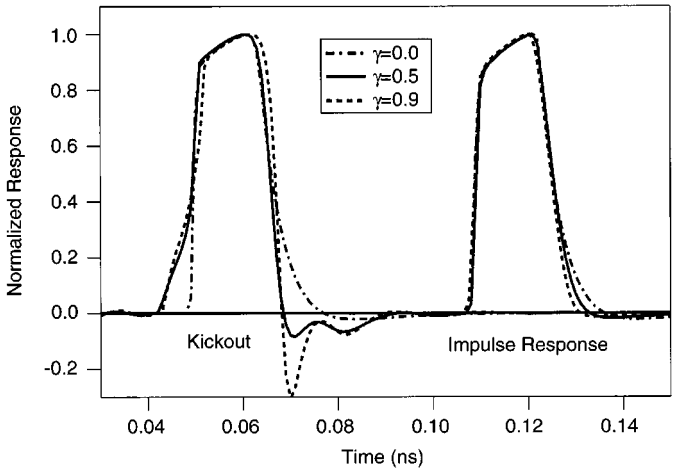

Fig. 3. Kickout and impulse response waveforms for increasing nonlinearity in the diode's junction capacitance. The impulse response has been shifted in time for clarity.

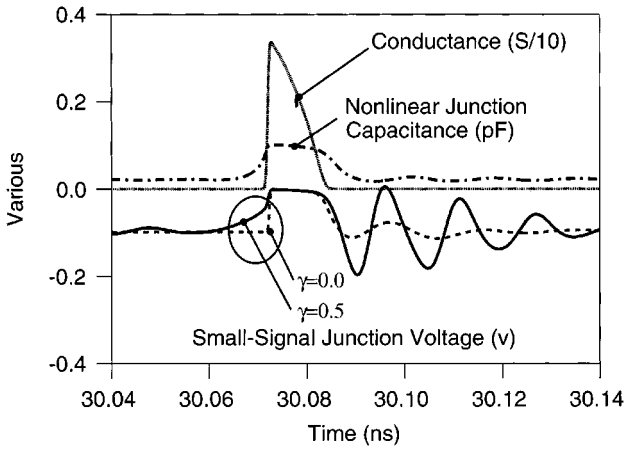

Fig. 4. Small-signal junction voltage with (solid) and without (dashed) nonlinear capacitance included in the SPICE model. The small-signal diode conductance (dots) and junction capacitance (dash-dots) are included for reference. For the case with $\gamma = 0.0$, the junction capacitance (not shown) is a constant of $C_{j0} = 0.045$ pF.

shown in Fig. 2 can be explained by looking at the kickout and impulse response waveforms in the time domain. Fig. 3 shows that the kickout waveform rise-times and fall-times are affected by the increase in nonlinear capacitance, while we see only a minimal change in the impulse response waveform.

IV. Small-Signal Model

The broadening of the kickout pulse shown in Fig. 3 can be explained by considering the components of the small-signal current in the sampling diodes. For the diode model described above, the equation for the small-signal current in the diode is [6]

$$i(t) = g(t)v_j(t) + v_j(t)\frac{dc(t)}{dt} + c(t)\frac{dv_j(t)}{dt}. \qquad (4)$$

Here $g(t)$ is the small-signal diode conductance, $c(t)$ is the diode's junction capacitance, equivalent to $C(V_j)$ in (3) [9], and $v_j(t)$ is the small-signal junction voltage.

Fig. 4 shows the small-signal junction voltage, v_j, with nonlinear junction capacitance ($\gamma = 0.5$, solid curve) and with constant junction capacitance ($\gamma = 0.0$, dashed curve). This latter case is nonphysical but its impact can be assessed using SPICE. For the constant-capacitance case, v_j changes only when the diode starts to conduct, as shown in the highlighted area of Fig. 4. For the case with $\gamma = 0.5$, v_j changes as the nonlinear capacitance changes. As shown by the second and third terms in (4), the time-varying quantities $c(t)$ and $v_j(t)$ give rise to a small-signal displacement current. This current causes the kickout pulse to broaden with nonlinear junction capacitance. Note that any time-varying capacitance in the sampling circuit would cause a similar effect.

The reason that the impulse response does not broaden can be understood by realizing that the kickout pulse is proportional to the instantaneous charge on the hold capacitors, while the impulse response is reconstructed from digitized samples, each of which is generated over one complete sampling cycle. The net charge transferred to the hold capacitors through the diode capacitance over one complete sampling cycle must be zero, since no conduction current path exists through the capacitance. A new analytic model supports this conclusion [6].

V. Conclusion

The broadening of the kickout pulse due to an increase nonlinearity of the sampling diode's junction capacitance has been explained using a small-signal model of the diode current. While this error is not corrected in current nose-to-nose calibration methods, its effects may be correctable by other means and are the subject of current research.

References

[1] K. Rush, S. Draving, and J. Kerley, "Characterizing high-speed oscilloscopes," *IEEE Spectrum*, pp. 38–39, Sept. 1990.
[2] J. Verspecht and K. Rush, "Individual characterization of broadband sampling oscilloscopes with a nose-to-nose calibration procedure," *IEEE Trans. Instrum. Meas.*, vol. 43, pp. 347–354, Apr. 1994.
[3] J. Verspecht, "Broadband sampling oscilloscope characterization with the 'nose-to-nose' calibration procedure: a theoretical and practical analysis," *IEEE Trans. Instrum. Meas.*, vol. 44, pp. 991–997, Dec. 1995.
[4] D. F. Williams, K. A. Remley, and D. C. DeGroot, "Nose-to-nose response of a 20-GHz sampling circuit," in *Proc. 54th ARFTG Conf. Dig.*, Atlanta, GA, Dec. 1999, pp. 64–70.
[5] P. D. Hale, T. S. Clement, K. J. Coakley, C. M. Wang, D. C. DeGroot, and A. P. Verdoni, "Estimating the magnitude and phase response of a 50 GHz sampling oscilloscope using the "Nose-to-Nose" method," in *Proc. 55th ARFTG Conf. Dig.*, Boston, MA, June 2000, pp. 35–42.
[6] D. F. Williams and K. A. Remley, "Analytic model for a sampling circuit," *IEEE Trans. Microwave Theory Tech.*, to be published.
[7] S. Riad, "Modeling of the HP-1430A feedthrough wideband (28-ps) sampling head," *IEEE Trans. Instrum. Meas.*, vol. IM-31, pp. 110–115, June 1982.
[8] K. A. Remley, D. F. Williams, and D. C. DeGroot, "Realistic sampling-circuit model for a nose-to-nose calibration," in *Proc. IEEE MTT-S Int. Microwave Symp. Dig.*, Boston, MA, 2000, pp. 1473–1476.
[9] S. A. Maas, *Microwave Mixers*, 2nd ed. Boston, MA: Artech House, 1993.